Influence of Structure on the Spectroscopic Properties of the Polymorphs of Piroxicam

Wei Liu,[†] Wei David Wang,[†] Wei Wang,[†] Shi Bai,*[,†,‡] and Cecil Dybowski[‡]

State Key Laboratory of Applied Organic Chemistry, Lanzhou University, Lanzhou, Gansu, 730000, China, and Department of Chemistry and Biochemistry, University of Delaware, Newark, Delaware 19716, United States

Received: September 4, 2010; Revised Manuscript Received: October 27, 2010

The complete ^{13}C NMR chemical-shift tensors for the carbon sites of the two polymorphic forms ($\mathbf{P_I}$ and $\mathbf{P_{II}}$) and the monohydrate form (**PM**) of the analgesic drug, piroxicam, are reported. The NMR parameters (isotropic chemical shifts, chemical-shielding anisotropies and asymmetries, and dipolar couplings), X-ray powder diffraction, and density functional calculations of piroxicam are analyzed in terms of hydrogen bonding and structure. The integration of all the data gives an improved model of the local solid-state structures of the polymorphs. In particular, the solid-state NMR spectra demonstrate that the asymmetric unit of the monohydrate, **PM**, contains two zwitterionic piroxicam molecules.

Introduction

The structure, locally and long-range, of a pharmaceutical solid is a critical parameter that affects quality, stability, safety, and efficacy of pharmaceutical products.[1] Various polymorphic forms of certain substances may, for example, have quite different apparent solubilities, dissolution rates, and bioavailability.[2] These differences affect the manner in which the pharmaceuticals are used in drugs and determine the types of formulations in which they are administered. Polymorphic forms may interconvert during storage,[3] limiting the shelf life of drugs that rely on the material being in a particular form. Understanding solid-state structure of these materials at local and long-range levels is key to developing strategies for the use of these drugs, and spectroscopic analysis provides the means to specify structure.

Piroxicam is a long-acting, nonsteroidal, analgesic drug used in the treatment of osteoarthritis and rheumatoid arthritis.[4] It exists in at least two polymorphic solid forms and as a monohydrate. It is the active ingredient in Feldene, a drug commercially available in the United States and Europe; and in Roxam, a drug commercially available in Africa, the Middle East, Asia, and parts of Europe. As the active constituent of these drugs, piroxicam is a model of the effects of polymorphism, particularly for pharmaceutical applications.[5]

The solid-state structure of piroxicam has been investigated with X-ray powder diffraction,[6,7] vibrational and Raman spectroscopy,[8−10] thermal analysis,[11,12] and, recently, solid-state NMR spectroscopy.[13−15] Two polymorphs of piroxicam that have been consistently identified are labeled $\mathbf{P_I}$ and $\mathbf{P_{II}}$, and their crystal structures have been reported.[14,16] Both are monoclinic and exist in space group $P2_1/c$. A third polymorph has been reported to form under certain conditions of recrystallization.[5,14] Piroxicam monohydrate, **PM**, is formed when piroxicam is recrystallized from aqueous solution. X-ray structures[17,18] of **PM** indicate that it has two molecules per asymmetric unit in the space group $P\bar{1}$, whereas $\mathbf{P_I}$ and $\mathbf{P_{II}}$ have only one molecule per asymmetric unit.

The molecular structure of the neutral form of piroxicam is shown in Figure 1a, and the zwitterionic form is shown in Figure 1b. The $\mathbf{P_I}$ and $\mathbf{P_{II}}$ forms of the native molecule are presumed to differ only in lattice energies, with the molecular conformational energies being similar.[5] Although the conformational energies are thought to be similar, $\mathbf{P_I}$ and $\mathbf{P_{II}}$ have slightly different ways in which hydrogen bonds are formed.[5] The neutral molecular structure may be converted into the zwitterionic form by a solid-state transfer of the hydroxyl proton on C7 to produce the pyridinium center at N3.[13] This process is usually accompanied by a change from the colorless crystal form to the yellow zwitterionic form.[13] In the hydrate, the conformation of the piroxicam structure is different from that of $\mathbf{P_I}$ and $\mathbf{P_{II}}$,[18] and it is presumed to exist predominantly as a zwitterion.

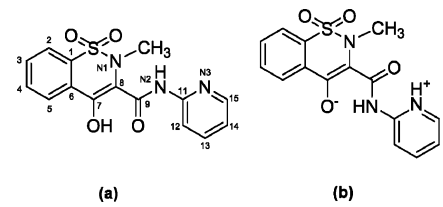

Figure 1. The molecular structure of piroxicam, showing the numbering of the carbons and nitrogens: (a) neutral form and (b) zwitterionic form.

Solid-state NMR (SSNMR) spectroscopy is an effective method to explore polymorphism in systems such as pharmaceutical substances.[19−28] The NMR chemical shielding is especially sensitive to molecular conformation as well as state of ionization. Dipolar couplings between nuclei, when measured, give direct information on internuclear distances that can be used to infer local structural features. The temperature dependence of relaxation and spectroscopic parameters such as chemical-shift tensors have been used to infer local dynamics.

The literature on the solid-state NMR spectroscopy of the polymorphs of piroxicam is sparse.[13−15] In one study,[13] the substantial isotropic deshielding of the ^{13}C resonance of C7 of **PM** relative to that of $\mathbf{P_I}$ and $\mathbf{P_{II}}$ was interpreted as evidence for the existence of the zwitterionic form of **PM**. In another study, differences in isotropic ^{13}C chemical shifts among the polymorphs were suggested as evidence for modes of hydrogen bonding.[14] More recently, an NMR study of a cocrystal of piroxicam with saccharin was consistent with piroxicam's being a zwitterion in the complex.[15] Most notably, in that study, the

* Corresponding author. E-mail: baishi@lzu.edu.cn or bais@udel.edu.
[†] Lanzhou University.
[‡] University of Delaware.

10.1021/jp1084444 © 2010 American Chemical Society
Published on Web 11/18/2010

principal values of some ^{13}C chemical-shift tensors provided critical evidence of differences between a polymorph and a complex, whereas the differences in isotropic chemical shifts were relatively small.

We report the complete assignments of the ^{13}C chemical-shift tensors of **P$_I$**, **P$_{II}$**, and **PM**. Along with the X-ray data, the NMR parameters of **PM** lead to a more refined model of the hydrogen-bonding network in that material. The analysis requires multiple techniques, including traditional ^{13}C CP/MAS spectra and spectra determined with suppression of nonquaternary carbon resonances.[29] To address structural features, contact-time-dependent, two-dimensional, heteronuclear correlation spectroscopy (2D-HETCOR) gave qualitative information on internuclear distances in the various polymorphs.

Because X-ray crystallographic studies can have difficulty locating hydrogen positions in some cases, one must determine those in some other manner. The commonly accepted structure of **PM** assumes a maximum H···A distance of 3.0 Å and a minimum D−H···A angle of 90° in the hydrogen-bonding network, together with the X-ray structure of the framework.[30] 2D-HETCOR spectroscopy can suggest limits on positions of hydrogens. In this study, we use these data and the X-ray data to propose a more refined model of hydrogen bonding in **PM**.

The complete experimental NMR results suggest that isotropic ^{13}C chemical shifts, although providing data that generally distinguish the polymorphs of piroxicam, are not as sensitive to subtle structural details as are the principal values of the chemical-shift tensor (CST). The CST reflects the three-dimensional electronic structure in the neighborhood of the nuclear site, which makes its full analysis a sensitive probe of local structure and molecular conformation. To examine this connection between structure and spectroscopic parameters, we performed density functional theory calculations with gauge invariant atomic orbitals (GIAO/DFT) to predict the manner in which the principal values of the CST change with conformation of the piroxicam structure. From these calculations, we have isolated the conformational contributions to the chemical-shift principal values at certain carbon sites. The results are consistent with the idea that **P$_I$** and **P$_{II}$** have similar conformations but that **PM** exists in a different conformation. The NMR data also imply that **PM** is zwitterionic, with intermolecular hydrogen bonding playing a key role in the structure.

Experimental Section

Sample Preparation. Piroxicam was purchased from Sigma (Lot no. 066K1779). Powder X-ray diffraction (PXRD) (see Figure S1 in the Supporting Information) demonstrated that the material, as received, was **P$_I$**, the most stable polymorph of piroxicam at ambient conditions. **P$_{II}$** was obtained from **P$_I$** by recrystallization from absolute ethanol.[5] **PM** was prepared from either **P$_I$** or **P$_{II}$** by water-mediated solid-state conversion at room temperature.[30] A sample of **PM** prepared with deuterium oxide (**PM-d**) was generated by the same procedure. PXRD data of **P$_I$**, **P$_{II}$**, and **PM** were essentially identical to those reported in the literature.[30] ^{13}C CP/MAS NMR spectra of the samples (Figure 2) gave isotropic chemical shifts that were nearly identical to those reported by Sheth et al.[13]

NMR Spectroscopy. CP/MAS experiments were carried out with a Bruker Avance II WB400 NMR spectrometer operating at a proton frequency of 400.13 MHz. Samples were packed in 4-mm rotors; a CP/MAS double-resonance (^{13}C and H) probe was used, and all spectra were obtained at 298 ± 2 K. CP/MAS experiments were carried out with a sample spinning rate of 10 000 ± 2 Hz. TPPM[31] decoupling during CP/MAS data

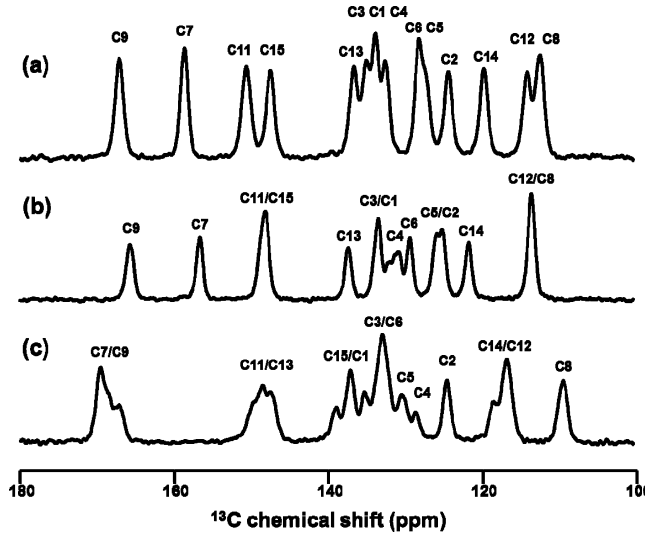

Figure 2. ^{13}C CP/MAS spectra of the structural forms of piroxicam: (a) **P$_I$**, (b) **P$_{II}$**, and (c) **PM**. Contact time: 3 ms.

acquisition was provided by a 104.2-kHz proton decoupling field. For most CP/MAS spectra, the contact time was 3 ms. For CP/MAS experiments carried out with nonquaternary carbon suppression,[29] a 40-μs delay was used to suppress the contributions of carbons adjacent to protons. All ^{13}C chemical shifts are referenced externally via the resonance of adamantane at an isotropic chemical shift relative to tetramethylsilane (TMS) of 38.55 ppm.

2D-HETCOR experiments[32] were performed with a spinning rate of 12 000 ± 2 Hz on the same instrument. The TPPM decoupling field strength was 104.2 kHz, with a pulse delay of 3.0 s. A Lee−Goldburg $^1H-^1H$ decoupling scheme[33,34] was used during the evolution period, which consisted of a 2.4-μs $\pi/2$ ^1H pulse and four Lee−Goldburg cycles per evolution increment. A total of 256 evolution points, each with either 96 or 128 scans, was collected. A series of data sets with cross-polarization times of 100, 200, 300, 500, 800, and 1000 μs were acquired. The ^1H dimension was referenced internally to the methyl group of piroxicam at 3.0 ppm, as determined with ^1H MAS NMR spectroscopy. The ^{13}C dimension was referenced externally to the resonance of adamantane at 38.55 ppm. All reported proton shifts were scaled by 0.578, the scaling expected for Lee−Goldburg homonuclear decoupling. The data were processed by multiplication by a cosine-square function in the t_1 and t_2 dimensions prior to Fourier transformation.

Determination of the CST for ^{13}C in multicarbon molecules allows one to see the three-dimensional effects of electronic structure at each unique site.[35−38] To determine CSTs of the piroxicam materials, we used the 2D-SUPER experiment.[38] In a typical 2D-SUPER experiment, the sample was spun at a frequency of 5000 ± 2 Hz, which dictates the 2π pulse lengths for chemical-shift recoupling. The proton decoupling amplitude during the recoupling section of the experiment was 116.8 kHz. For each t_1 increment, 2048 complex points were collected along the acquisition (isotropic) dimension. Depending on the signal-to-noise ratio, either 256 or 512 scans were coadded; 32 complex points along the F_1 (anisotropic) dimension were used. The recoupling section was followed by a γ-integral delay of 1 ms to eliminate spinning sidebands in the F_1 dimension. A TOSS sequence[39,40] was used to suppress spinning sidebands in the F_2 dimension. The scaling factor for the SUPER experiment was 0.155.

A cosine-square function was applied to both the t_1 and t_2 dimensions prior to Fourier transformation. Subsequently,

TABLE 1: Principal Values of the ^{13}C Chemical-Shift Tensors of the Polymorphs of Piroxicam and Piroxicam Monohydrate[a]

	P_I					P_{II}					PM				
C#	δ_{11} (ppm)	δ_{22} (ppm)	δ_{33} (ppm)	δ_{iso} (ppm)	δ_{iso}[b] (MAS) (ppm)	δ_{11} (ppm)	δ_{22} (ppm)	δ_{33} (ppm)	δ_{iso} (ppm)	δ_{iso}[b] (MAS) (ppm)	δ_{11} (ppm)	δ_{22} (ppm)	δ_{33} (ppm)	δ_{iso} (ppm)	δ_{iso}[b] (MAS) (ppm)
1	209 (202)[c]	149 (157)	43 (49)	134 (136)	133.6	212 (204)	152 (159)	36 (55)	133 (139)	133.3	207 (202)[d]	156 (161)	43 (55)	135 (139)	135.0
2	227 (214)	141 (140)	5 (8)	124 (121)	124.1	222 (214)	157 (141)	−3 (8)	125 (121)	125.0	220 (214)	149 (138)	4 (9)	124 (120)	124.2
3	223 (226)	152 (145)	30 (5)	135 (125)	134.8	245 (229)	124 (147)	30 (4)	133 (127)	133.3	253 (227)	149 (143)	−4 (6)	133 (125)	132.6
4	235 (225)	156 (142)	6 (5)	132 (124)	132.3	[e] (229)	[e] (144)	[e] (4)	[e] (126)		230 (225)	153 (140)	3 (7)	128 (124)	128.4
5	229 (216)	159 (149)	−7 (4)	127 (123)	127.2	223 (218)	156 (149)	−2 (3)	126 (123)	125.7	237 (220)	152 (149)	1 (3)	130 (124)	130.2
6	216 (201)	163 (158)	5 (27)	128 (129)	127.9	218 (201)	164 (158)	6 (28)	129 (129)	129.2	213 (209)	165 (163)	20 (31)	133 (135)	132.6
7	248 (234)	162 (169)	65 (81)	158 (162)	158.5	247 (231)	161 (167)	62 (77)	157 (158)	156.5	255 (249)	186 (182)	67 (78)	169 (169)	169.4
8	176 (165)	104 (108)	56 (63)	112 (112)	112.1	176 (167)	103 (115)	60 (66)	113 (116)	113.4	160 (154)	98 (107)	69 (73)	109 (111)	109.0
9	245 (228)	173 (160)	83 (102)	167 (163)	167.0	244 (231)	164 (161)	90 (104)	166 (165)	165.7	242 (226)	163 (151)	96 (112)	167 (163)	167.0/168.4
11	252 (237)	145 (136)	54 (67)	150 (147)	150.4	241 (239)	138 (138)	67 (66)	148 (148)	148.0	224 (197)	175 (162)	50 (64)	149 (141)	149.4/147.8
12	200 (195)	138 (128)	4 (8)	114 (111)	113.9	201 (196)	129 (128)	10 (9)	113 (111)	113.4	218 (191)	137 (121)	−6 (22)	116 (111)	116.4
13	245 (234)	170 (151)	−6 (2)	136 (129)	136.4	245 (237)	164 (154)	3 (3)	137 (131)	137.2	232 (240)	168 (158)	41 (3)	147 (134)	147.1/148.5
14	228 (216)	128 (120)	3 (6)	120 (114)	119.5	229 (218)	128 (122)	7 (6)	121 (121)	121.4	213 (206)	135 (122)	7 (7)	118 (112)	118.2
15	245 (245)	142 (151)	55 (36)	147 (145)	147.2	261 (248)	148 (152)	35 (39)	148 (147)	148.0	237 (221)	154 (155)	26 (35)	139 (137)	138.8/137.2

[a] The uncertainty of chemical shift tensor components is estimated to be ±3 ppm. [b] Isotropic values from CP/MAS experiments with a uncertain of ±0.1 ppm. [c] Data in parentheses are calculated results using the ADF package, as described in text. [d] ADF calculations for **PM** are based on CIDYAP01 structure file with proton transfer. [e] It is difficult to obtain accurate tensor components for C4 of $\mathbf{P_{II}}$ because of its multiple-resonance characteristics.

spectra were repeatedly sheared along the F_1 dimension until the anisotropic chemical-shift patterns were centered in the spectrum along the F_1 dimension. To determine the CST fully, the appropriate spectral slice was fitted with the line-shape-analysis package of Bruker's TopSpin software. The referencing of the extracted chemical-shift pattern was based on its corresponding isotropic shift in the F_2 dimension.

When isotropic chemical shifts of two resonances were sufficiently close that the patterns overlapped (such as C1/C3, C8/C12, and C11/C15 in $\mathbf{P_{II}}$), DD-SUPER[41] was used to isolate the patterns of the unprotonated carbons. Fitting of the ^{13}C powder pattern of an unprotonated carbon allowed us to fix the parameters of this contribution when fitting the full 2D-SUPER powder pattern of the same sample. During this latter fitting, only the CST parameters of the protonated carbons were variables, which allowed precise determination of the overlapped powder patterns.

Computational Methods. The crystal structures of the polymorphs of piroxicam (BIYSEH[16] for $\mathbf{P_I}$, BIYSEH05[14] for $\mathbf{P_{II}}$, and CIDYAP01[18] for **PM**) from the Cambridge Structure Database (CSD) were used in the GIAO/DFT calculations without further geometry optimization, except that we optimized the hydrogen positions. The principal values of the NMR CSTs and the total molecular energies were determined with the Amsterdam Density Functional (ADF) software package,[42−45] using a valence double-ζ Slater-type basis set with polarization functions. In the ADF calculations, the local density approximation and the generalized gradient approximation were used in the SCF procedures.

Similar calculations were also performed with the Gaussian 03 software package[46] at the B3PW95 level of theory with the 6-311++G(2p, d) basis set, which gave similar results. A comparison of the principal values of the NMR CSTs between ADF and Gaussian 03 for piroxicam is given in Table S1 in the Supporting Information. The calculated ^{13}C chemical-shift parameters were referenced to the isotropic position of TMS, obtained at the same level of theory and with the same basis sets.

Powder X-ray Diffraction. X-ray diffraction patterns of powdered $\mathbf{P_I}$, $\mathbf{P_{II}}$, and **PM** were recorded for 2θ between 5° and 50° with a Rigaku D/Max 2400 powder-diffraction system, using Cu Kα radiation at 298 K. The PXRD data are given in Figure S1 in the Supporting Information.

Results and Discussion

Isotropic ^{13}C NMR Spectral Assignments. The isotropic ^{13}C chemical shifts of $\mathbf{P_I}$, $\mathbf{P_{II}}$, and **PM** in deuterated chloroform solution are identical (data not shown). The conformation of the piroxicam moiety in solution is therefore independent of the structure and molecular conformation of the solid form from which the solution is made. The isotropic ^{13}C chemical shifts of the solutions are close to those of solid $\mathbf{P_I}$ determined with CP/MAS spectroscopy. This similarity between solution and solid-state NMR parameters suggests that the average solution conformation and the conformation of solid $\mathbf{P_I}$ are similar, and that this is the lowest-energy conformation.

The regions of the CP/MAS ^{13}C NMR spectra between 100 ppm and 180 ppm of solid $\mathbf{P_I}$, $\mathbf{P_{II}}$, and **PM** are shown in Figure 2. The ^{13}C isotropic chemical shifts of the three forms of piroxicam indicate that the materials vary in structure, with the spectrum of **PM** deviating significantly from those of the two polymorphs. There are also systematic differences between the spectra of $\mathbf{P_I}$ and $\mathbf{P_{II}}$, suggesting the influence of structure on the NMR parameters.

Because of severe overlap of resonances in the spectra of $\mathbf{P_{II}}$ and **PM**, only partial resonance assignments have been previously reported.[13] Figure 2 indicates that there is substantial overlap of at least three pairs of ^{13}C resonances (C11/C15, C1/C3, and C8/C12) of $\mathbf{P_{II}}$. The complete assignments in Table 1 for $\mathbf{P_{II}}$ and **PM** are possible through a comparison of the CP/MAS spectra with the CP/MAS spectra obtained with suppression of signals from nonquaternary carbons. (Figures S2 and S3 in the Supporting Information).

A distinguishing feature of these spectra is the deshielding of the resonance of C7 in **PM** relative to the resonances of C7 in $\mathbf{P_I}$ and $\mathbf{P_{II}}$. Sheth et al. attribute this difference to a change in structure due to proton transfer.[13] A further difference is the noticeably broader resonances of certain carbon sites (C7, C9, C11, C13) in **PM**. This broadening is not likely to be the result of the presence of amorphous phases because it is well-known from PXRD measurements that **PM** is predominantly crystalline. As we discuss later, such broadening is more likely evidence of the existence of more than one molecule in the asymmetric unit in **PM**, giving a slight dispersion to the chemical shift.

A measure of the difference between the spectra of two similar compounds is the total combined root-mean-squared

deviation (rmsd) of the isotropic chemical shifts. A comparison of the monohydrate to the two polymorphs gives rmsd's of 1.4, 5.2, and 5.6 ppm for $\mathbf{P_I}/\mathbf{P_{II}}$, $\mathbf{P_I}/\mathbf{PM}$, and $\mathbf{P_{II}}/\mathbf{PM}$, respectively. These deviations indicate that the electronic environments of $\mathbf{P_I}$ and $\mathbf{P_{II}}$ are, on average, quite similar, whereas both are noticeably different from the electronic environment of the monohydrate. A closer examination of the isotropic chemical shifts of specific carbons indicates that the rmsd's reflect changes in chemical shifts of sites such as C7, C13, and C15.

The differences in isotropic rmsd's may result from differences in conformation, differences in ionization state, or differences in molecular packing. As such, they reflect the contributions of differences in conformational energies, ionization behavior, and lattice energies. One might therefore reasonably assume that measures of these quantities correlate with the rmsd's.

The conformational energy is readily obtained from DFT calculations on known crystallographic structures.[47] We carried out calculations to obtain qualitative conformational energies of structures of $\mathbf{P_I}$, $\mathbf{P_{II}}$, and **PM** (BIYSEH, BIYSEH05, and CIDYAP01) obtained from the CSD, using the ADF software package. (Some calculations with Gaussian 03 showed analogous results.) For the **PM** structure, because there are no hydrogens reported in CIDYAP01, hydrogens were added to the structure, and their positions were optimized using the ADF software package.

The results predict that $\mathbf{P_I}$ is the lowest-energy structure, with $\mathbf{P_{II}}$ being only slightly higher. The monohydrate is significantly higher in energy. ($E_{ADF}(\mathbf{P_{II}}) - E_{ADF}(\mathbf{P_I}) \sim 1.5$ kJ/mol and $E_{ADF}(\mathbf{PM}) - E_{ADF}(\mathbf{P_I}) \sim 36$ kJ/mol; $E_{G03}(\mathbf{P_{II}}) - E_{G03}(\mathbf{P_I}) \sim 0.95$ kJ/mol and $E_{G03}(\mathbf{PM}) - E_{G03}(\mathbf{P_I}) \sim 40$ kJ/mol.) These results are comparable in magnitude to previous calculations of the conformational energy differences in other polymorphic systems.[21,47,48] At least for the three piroxicam structures, the ^{13}C isotropic chemical shift rmsd's do seem to be correlated with conformational-energy differences, suggesting that the differences in isotropic NMR chemical shifts are the result of conformational differences.

Structure of the Asymmetric Unit of Piroxicam Monohydrate. X-ray crystallographic structures of **PM** indicate that the asymmetric unit contains two piroxicam molecules ($Z' = 2$).[18] To date, the ^{13}C NMR CP/MAS spectra of **PM** have been interpreted in terms of a single piroxicam molecule (or symmetrically related molecules) in the asymmetric unit. The line-broadening observed in the CP/MAS spectrum of **PM** (Figure 2c) is suggestive of overlap of resonances from molecules at sites that have slightly different local electronic environments. To investigate the line broadening further, ^{13}C−^{1}H HETCOR spectra of **PM** were acquired as a function of contact time (100 μs < t_c < 1000 μs). Figure 3 shows the ^{13}C−^{1}H HETCOR spectrum of **PM** taken with a contact time of 500 μs, in which the cross-peaks are labeled. The proton resonance assignments for N2**H** and N3**H**$^+$ follow the work of Vogt et al.[15] The peak at 15.4 ppm is assigned to N2**H**, and the peak at 14.3 ppm, to N3**H**$^+$. These assignments are in reasonable agreement with the predicted trend of isotropic chemical shifts by the ADF calculations (17.3 ppm for N2**H** and 16.6 ppm for N3**H**$^+$).

Once the isotropic proton chemical shifts of N2**H** and N**H**3$^+$ are fixed, the resonance at 12.7 ppm can be assigned to the protons of the water of hydration. An isotropic chemical shift of 12.7 ppm may seem higher than shifts commonly reported for water. However, the isotropic shift of water in hydrogen-bonded hydrates ranges for 4.8 ppm to 10.4 ppm, depending on the strength of the hydrogen bonding in which the water is involved.[49] In the case of zwitterionic piroxicam monohydrate, it is conceivable that these hydrogen-bonded water protons may be subject to strong deshielding, resulting in the appearance of these protons at the edge of this range. A ^{2}H MAS spectrum of the sample **PM-d** (Figure S4 in the Supporting Information), prepared by dripping D_2O on piroxicam, shows centerband resonances ranging only from 10.8 to 16.6 ppm. No signal with positions at chemical shifts less than 10.8 ppm was observed, supporting the assignment of the water resonance. The cross-peaks in the correlation spectrum in Figure 3 are somewhat tilted toward the shielded end in both the ^{1}H and ^{13}C directions. This may also be a result of the inhomogeneity due to the anisotropy of the bulk magnetic susceptibility of the sample.[50,51]

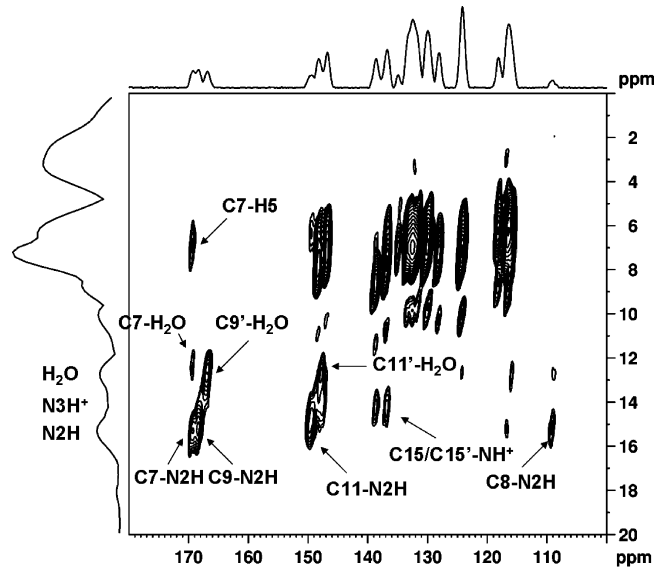

Figure 3. A portion of ^{13}C−^{1}H HETCOR spectrum of **PM**. Contact time: 500 μs. The labeled cross-peaks are explained in the text. The unlabeled cross-peaks with ^{1}H chemical shifts between 4 and 10 ppm and with ^{13}C chemical shifts <150 ppm arise from aromatic carbon and proton correlations.

The ^{13}C projections of the 2D-HETCOR spectra are given in Figure 4, where the ^{13}C signals represent carbons coupled to protons through dipolar interactions. At short contact times, only signals of carbons directly bonded to hydrogen (such as in a C−H bond) appear in these projected spectra. At longer contact times, particularly for contact times of 1000 μs or more, spin-diffusion may result in HETCOR projections that resemble the CP/MAS spectrum of Figure 2c. For **PM**, spectra taken with contact times less than 200 μs show two pairs of resonances having nearly equal intensities for C13/C13′ (148.5/147.1 ppm) and C15/C15′ (138.8/137.2 ppm). For a contact time of 300 μs, a pair of cross-peaks of C9/C9′ appears at 169.4/167.0 ppm in the 2D-HETCOR spectrum. A similar splitting of the C11 resonance is seen in the CP/MAS spectrum (Figure S3 of the Supporting Information) taken with suppression of nonquaternary carbons. This doubling of resonances is clearly suggestive of the existence of two piroxicam molecules in the asymmetric unit of **PM**, in agreement with X-ray data, something that is only hinted at by broadening in the CP/MAS spectra.

The appearance of signals in the 2D-HETCOR spectra at longer contact times implies the existence of weaker dipolar couplings to protons at greater distances. At 300 μs, the signal of the resonance of the unprotonated C1 appears as a shoulder on the C15 resonance. We attribute the appearance of this feature to dipolar coupling between C1 and H2, even though C1 and H2 are *not* directly bonded. Although not unambiguously

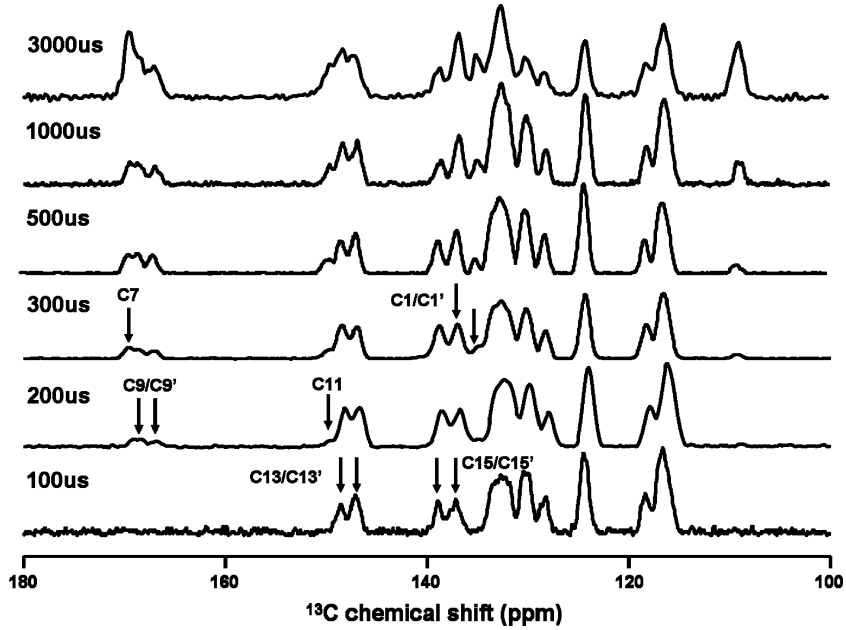

Figure 4. ^{13}C projections of 2D HETCOR spectra of **PM** as a function of contact time. The top trace (contact time: 3000 μs) is a CP/MAS spectrum, presented for comparison.

resolved in the 2D-HETCOR spectrum, a C1′ signal underlies the resonances of C15 and C15′. The growth of this C1′ resonance with contact time is reflected in the deviation of the C15-to-C15′ intensity ratio from 1 as the contact time increases. The C1 and C1′ resonances can be more clearly discerned in the CP/MAS spectrum of **PM** obtained with nonquaternary-spin suppression (Figure S3 in the Supporting Information).

Not all carbons of piroxicam show detectable splitting of the resonance in the ^{13}C 2D-HETCOR projections. Most doubled resonances (C9, C11, and C15) are in regions of the molecule one expects to be affected by intermolecular and intramolecular hydrogen bonding. The doubled resonances of C9 and C11 are separated by only ~1 ppm, but they correspond to different HETCOR cross-peak patterns, indicating different hydrogen bonding and stereochemistry around these carbons sites.

NMR Evidence for Zwitterionic Piroxicam in the Monohydrate. The conformation of **PM**, as determined by X-ray diffraction, is different from those of $\mathbf{P_I}$ and $\mathbf{P_{II}}$. The significant difference in the isotropic shift of C7 of **PM** relative to $\mathbf{P_I}$ or $\mathbf{P_{II}}$ has been attributed to this conformational difference.[13] In addition, the piroxicam in **PM** is zwitterionic, the result of a net proton transfer from the hydroxyl group on C7 to the pyridine nitrogen (N3$\mathbf{H}^+$) on the oxicam group, which also affects the NMR shift of C7.

The 2D-HETCOR spectrum of **PM** acquired with a contact time of 500 μs (Figure 3) contains cross-peaks between the resonances of C15 and C15′ at 138.8/137.2 ppm and the proton resonance at 14.3 ppm, which is consistent with the assignment of the peak at 14.3 ppm to a labile hydrogen such as N3$\mathbf{H}^+$.[15] From models, one sees that the pyridinium center (N3H^+) is ~2.0 Å from C15/C15′. On the other hand, C15/C15′ is ~4.3 Å from N2**H**, a distance too great to show significant coupling in the 2D-HETCOR experiment. These results suggest that protonation occurs at N3, further evidence of zwitterionic behavior in **PM**. The increased isotropic shielding of C15/C15′ of **PM** (138.8/137.2 ppm) relative to that of $\mathbf{P_I}$ (147.2 ppm) or $\mathbf{P_{II}}$ (148.0 ppm) is also consistent with this assignment.

These couplings involve a labile hydrogen. A sample (**PM-d**) of **PM**, made by dripping D_2O on piroxicam, was also examined with the 2D-HETCOR experiment. The labile hydrogens should be replaced by deuterons via this procedure. The 2D-HETCOR spectrum of **PM-d** (Figure S5 in the Supporting Information) shows no cross-peaks between C15/C15′ and the proton resonance at 14.3 ppm, confirming that the resonance at 14.3 ppm is from a labile hydrogen. The observation of HETCOR cross-peaks between C7 and the hydroxyl proton on C7 in $\mathbf{P_I}$ and $\mathbf{P_{II}}$ (data not shown), and the lack of such a cross-peak in the **PM** spectrum also implies that the local structure of **PM** is quite different from those of $\mathbf{P_I}$ and $\mathbf{P_{II}}$. All of these observations and others[15] support the assignment of the resonances at 138.8 and 137.2 ppm to C15 and C15′.

Hydrogen Bonding in Piroxicam Monohydrate. The X-ray structure of **PM** shows two prioxicam molecules per asymmetric unit, but it does not show the hydrogen positions.[18] The structure with a high *R*-factor reported by Bordner et al.[17] was obtained at room temperature, limiting its ability to accurately locate hydrogen positions. A model of the hydrogen bonding in **PM** has been proposed by assuming a maximum H···A distance of 3.0 Å and a minimum D−H···A angle of 90°.[5,30] The model has four piroxicam molecules arranged as two dimers connected in a relatively planar structure through intermolecular hydrogen bonding to waters of hydration in a centrally located tetrameric structure. In this model, the hydrogen bonding occurs at the oxygen atom on C7 in the piroxicam structure.

NMR is particularly efficient at determining relative hydrogen positions from the magnitudes of dipole−dipole couplings. It qualitatively establishes structure by the appearance of dipolar couplings, which implies that the two nuclei are within ~3 Å. The 2D-HETCOR spectrum in Figure 3 shows a number of cross-peaks due to dipolar coupling that qualitatively establish maximum distances in the hydrogen-bonding network of **PM**. For example, a cross-peak at $\delta_C = 149.4$ ppm, $\delta_H = 15.4$ ppm indicates an intramolecular dipolar coupling between C11 and N2**H**, which have an internuclear distance of ~1.98 Å in the model. As another example, the cross-peak at $\delta_C = 147.8$ ppm, $\delta_H = 12.7$ ppm reveals an intermolecular coupling between C11′ of one molecule and a water proton. The cross-peak at $\delta_C = 169.4$ ppm, $\delta_H = 12.7$ ppm implies a dipolar coupling between C7 and the water protons, as a result of hydrogen bonding between the oxygen on C7 and a water molecule. The assign-

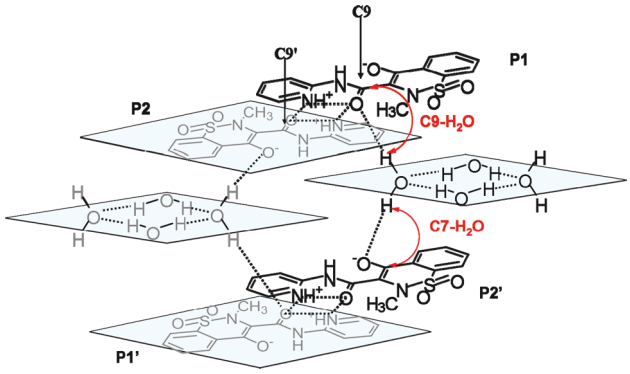

Figure 5. A model of hydrogen bonding in **PM** based on the analysis of $^{13}C-^{1}H$ HETCOR data. Red arrows indicate through-space correlations observed in the HETCOR spectra with contact time > 200 μs. Dashed lines represent hydrogen bonds. C9 in P1 and P1′ differ from C9′ in P2 and P2′ because of the involvement of water in hydrogen bonding to the carbonyl oxygens.

ment of C7 is reconfirmed by the existence of the cross-peaks linking C7 to H5 and to N2**H**, which have proton resonances of 6.9 ppm and 15.4 ppm, respectively.

The cross-peak between C9′ (δ_C = 166.8 ppm) and the water resonance at δ_H = 12.7 ppm shows that the oxygen on C9′ must also be involved in hydrogen bonding with the water tetramers. These data show that the two piroxicam dimers are connected by the water tetramers in different ways, as suggested by Sheth et al.[30]

The HETCOR data, in conjunction with the X-ray data, produce a somewhat refined model of the hydrogen-bonding network in **PM**. A nonplanar model consistent with these data is given in Figure 5. In this model, there are two types of C9 (C9 and C9′) in the dimer. The oxygen on C9 participates only in intramolecular hydrogen bonding to form the dimer. The second oxygen (C9′) also participates in hydrogen bonding with water. The validity of this structure is reinforced by the observation of separate resonances for C11 and C11′ in **PM**, which are similar to those observed for C9 and C9′.

The primary difference between Sheth's model and the model in Figure 5 is how the two dimers are connected. In Sheth's model, only the oxygen on C7 is involved in the hydrogen bonding to the water tetramers. In the proposed model, the NMR parameters suggest additional hydrogen bonding to the water through the oxygen at C9′. The diversity in the hydrogen-bonding structure is the key to stabilizing the hydrate structures in **PM**.

The ^{13}C Chemical-Shift Tensors of Piroxicam. The isotropic NMR chemical shift is an average of the three principal values of chemical shift tensor. The principal values, δ_{11}, δ_{22}, and δ_{33}, of the symmetric second-rank chemical-shift tensor (CST) provide more details about the electronic structure in three dimensions. There are a number of techniques for obtaining the principal values of the CST.[35,37,38,52] We used the 2D-SUPER[38] and DD-SUPER[41] techniques in this work. The experimental and predicted principal values of the CSTs of all the carbons of $\mathbf{P_I}$, $\mathbf{P_{II}}$, and **PM** are given in Table 1, along with the isotropic shifts as determined in CP/MAS experiments. The principal values for $\mathbf{P_I}$ recently reported by Vogt et al.[15] agree, at worst within 5 ppm, with the principal values for the carbons of $\mathbf{P_I}$ in Table 1.

The isotropic shifts of the carbons of $\mathbf{P_I}$ and $\mathbf{P_{II}}$ are quite close (rmsd = 1.4 ppm). On the other hand, the differences in the principal values of the CSTs for these two forms are significantly larger, with an rmsd of the entire set of principal values of 9.1 ppm. From X-ray analysis, the principal difference between $\mathbf{P_I}$ and $\mathbf{P_{II}}$ is packing within the crystal, which suggests that the principal values of the chemical-shift tensor are more sensitive to crystal packing than the isotropic values.

One cannot, in principle, generally determine the orientation of the principal axes in the molecular frame from NMR experiments on powders.[53] However, the orientations of the principal axes of the chemical-shift tensors of carboxyl and carbonyl carbons in the molecular frame are consistently observed to be related to the molecular frame. The 22 axis is nearly collinear with the direction of the double bond (C═O), and the 33 axis is perpendicular to the plane containing the C═O bond.[54−56] The 11 axis is perpendicular to the plane of these two axes.

The large rmsd of the isotropic chemical shifts of the carbons of $\mathbf{P_I}$ and **PM** must be attributed in part to the large isotropic deshielding of C7 in **PM** relative to C7 of $\mathbf{P_I}$. That large isotropic deshielding of C7 of **PM** relative to the others arises mainly from the fact that δ_{22} of C7 in **PM** is deshielded by ~25 ppm relative to δ_{22} of C7 in either $\mathbf{P_I}$ or $\mathbf{P_{II}}$. This shift results from the effects of deprotonation of the oxygen and the possibility of hydrogen bonding at this oxygen on C7, as depicted in Figure 5. In addition, a number of other carbons (C11, C13, C14, and C15) have differences in δ_{22} ≥10 ppm, when comparing **PM** with $\mathbf{P_I}$ or $\mathbf{P_{II}}$. These differences are most likely due to differences in the aromatic structure of the pyridine ring when it is protonated.

The δ_{22} of C9 of **PM** is 10 ppm *more* shielded than C9 of $\mathbf{P_I}$ (Table 1), which we ascribe to hydroxyl characteristics of C−O group in C9 in **PM**.[38] What is more interesting is that δ_{22} of C9 of $\mathbf{P_{II}}$ is shifted by almost the same amount from C9 in $\mathbf{P_I}$, even though the isotropic values for these two sites differ by only 1.4 ppm. This NMR observation suggests that hydrogen bonding at this site in $\mathbf{P_{II}}$ is more like that in **PM** than in $\mathbf{P_I}$. If so, then $\mathbf{P_I}$ and $\mathbf{P_{II}}$ are different principally as a consequence of subtly different hydrogen-bonding patterns.

Density Functional Theory Calculations of Piroxicam. The X-ray structures of piroxicam show that the monohydrate exists in a conformation very different from the two polymorphs.[14,16,18] One may interconvert the conformation of an unhydrated form to the hydrated form by a change of each of two dihedral angles by approximately 180°, as shown in Figure 6. For example, the conformation of $\mathbf{P_{II}}$ can be converted into that of **PM** by a change of the dihedral angle C7—C8—C9—O1 from 354.7° to 181.0° and by a change of the dihedral angle C9—N2—C11—N3 from 184.9° to 7°. One can envision numerous pathways to realize this change. We calculate the change in NMR parameters and energies along a particularly simple pathway to demonstrate how the CST depends on conformation.

A series of ADF DFT calculations were performed on conformations having various values of the dihedral angles, by systematically changing the angle incrementally by 10° along the pathway shown in Figure 6. Along this pathway, the dihedral angle C7—C8—C9—O1 of $\mathbf{P_{II}}$ was initially changed while holding the second dihedral angle fixed. Once the first dihedral angle reaches the value found for **PM**, subsequent systematic changes of the dihedral angle C9—N2—C11—N3 were made until it also achieved the value for **PM**. For each point along the pathway, the positions of the carbons, nitrogens, and oxygens were held constant as the hydrogen positions were optimized, with subsequent calculation of the NMR parameters.

The calculated isotropic ^{13}C chemical shifts of C6 (black), C7 (blue), C8 (red), and C9 (green) along the pathway are given in Figure 7. In this figure, solid symbols indicate the experi-

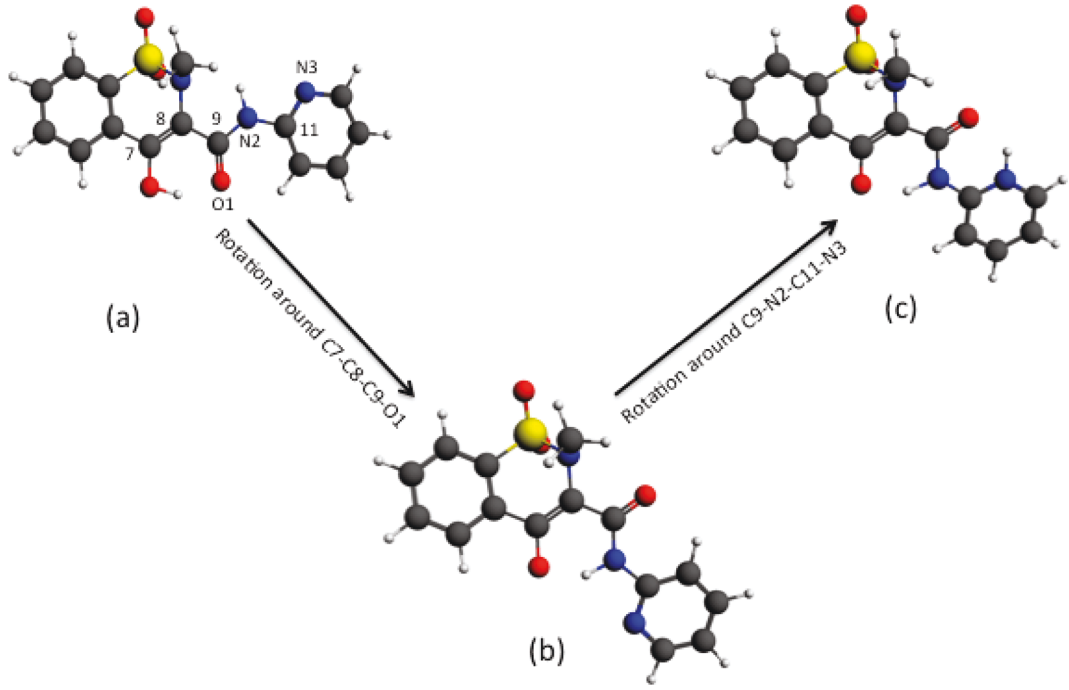

Figure 6. Dihedral rotations of piroxicam. The conformation of $\mathbf{P_{II}}$ is transformed into a **PM**-like conformation by a rotation around C8—C9, followed by a second rotation around N2—C11.

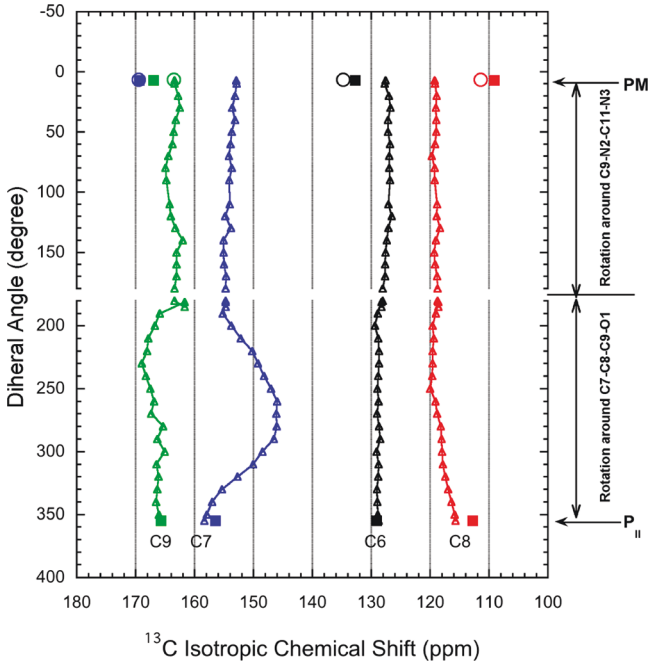

Figure 7. The variation of the isotropic ^{13}C chemical shifts as a function of dihedral angle for C6, C7, C8, and C9. The solid squares are the experimentally determined chemical of $\mathbf{P_{II}}$ and **PM**. The open circles represent the chemical shifts calculated from a conformer obtained by rotation of the $\mathbf{P_{II}}$ structure and hydrogen transfer to the nitrogen on the pyridine ring. Note the predicted strong variation of the isotropic shift of C7 as a function of the dihedral angle.

mental isotropic chemical shifts of $\mathbf{P_{II}}$ and **PM**. The open circles indicate the isotropic chemical shifts for conformers formed from $\mathbf{P_{II}}$ by the two dihedral rotations *and* by moving the hydrogen from the oxygen on C7 to protonate the pyridine at N3.

The calculated ^{13}C isotropic shifts of $\mathbf{P_{II}}$ agree well with the experimental shifts. On the other hand, change of conformation alone does not produce agreement between the calculated shifts and those of the monohydrate, **PM**. However, ADF calculations on a structure that includes a hydrogen transfer to N3 give much better agreement with experimental values for all carbon sites of **PM**. From these results, one concludes that conformational change alone does not account for the chemical-shift differences between the polymorphs and the monohydrate and that protonation at N3 has a major effect.

The change in the relative total energy of a conformation along this pathway is shown in Figure 8. The open square and the solid square represent the calculated relative energies of $\mathbf{P_{II}}$ and **PM**, respectively, using the X-ray structural parameters. For the energy of **PM**, the hydrogen transfer from the C7 hydroxyl group to N3 was carried out prior to the calculation of the energy. The open triangles show the change in the total energy as a function of the rotational angles that converts the structure of $\mathbf{P_{II}}$ to that of $\mathbf{P_M}$ without proton transfer. Once again, conformational changes alone do not account for the energy of the **PM** conformer. However, change of conformation *and* hydrogen transfer (shown as the solid triangle) produce an energy that is in much closer agreement with the prediction of **PM** determined with its experimental conformation. The energy difference between the **PM** and $\mathbf{P_{II}}$ rotamers (Figure 8) may be ascribed to crystal structure differences between **PM** and $\mathbf{P_{II}}$.

We point out that the relative energies in Figure 8 only represent changes in conformation and hydrogen transfer. This calculated energy does not reflect the energy benefit from hydrogen bonding due to the formation of the hydrate. In general, the hydrated forms of a drug are more stable than the anhydrates.

These calculations suggest the net transfer of a proton from the hydroxyl group on C7 to pyridine N3. This transfer stabilizes the piroxicam structure and promotes a significant redistribution of charge in piroxicam, which is reflected in the NMR chemical-shift parameters. For another polymorphic material, 5-methyl-2-[(2-nitrophenyl)amino]-3-thiophene carbonitrile (ROY), the chemical-shift variations of polymorphs are almost exclusively due to conformational changes.[25] In that case, the NMR shift variation does not require proton transfer, as for piroxicam.

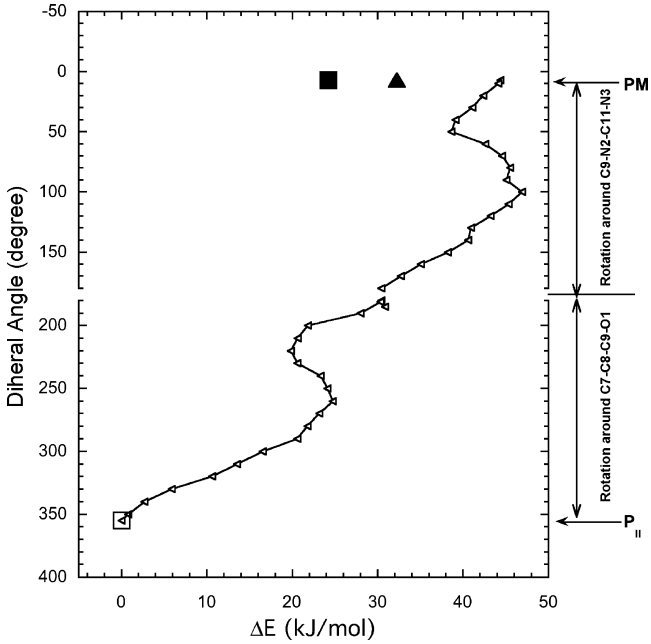

Figure 8. The calculated energy relative to $\mathbf{P_{II}}$ of piroxicam as a function of the two dihedral angles, starting from the structure of $\mathbf{P_{II}}$. The calculated relative energies of **PM** shown at the arrow are ■, based on the crystal structure of PM assuming proton transfer to the pyridinium center; abd ▲, based on the rotated structure of $\mathbf{P_{II}}$ with proton transfer.

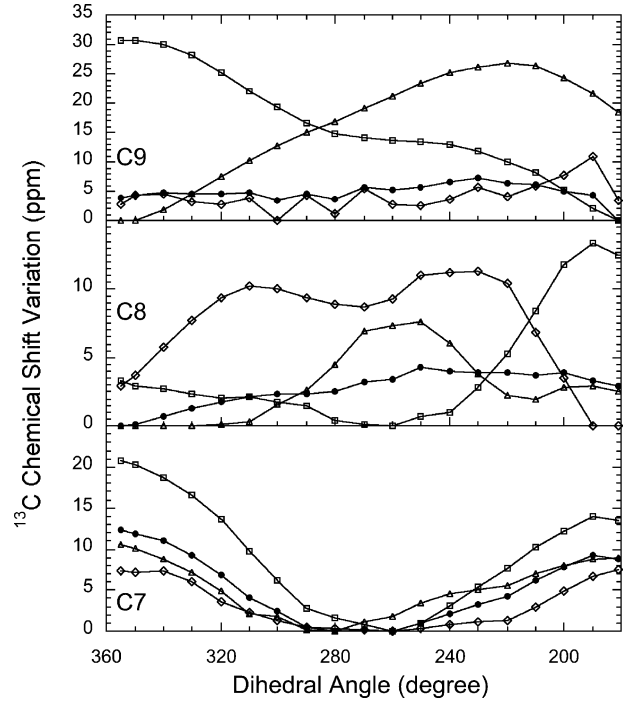

Figure 9. The calculated relative principal values of the ^{13}C chemical-shift tensors of C7, C8, and C9 as a function of the first dihedral angle (C7—C8—C9—O1), indicating that small changes in isotropic shifts are often the result of the cancellation of larger changes in the principal values. The exception to this is C7. The solid symbols show the isotropic chemical shift; the open symbols △, □, ◇, represent the principal values δ_{11}, δ_{22}, and δ_{33}, accordingly.

The variation of the *relative* principal values of the ^{13}C CST with the dihedral angles indicates how the electronic structure's geometry affects the chemical shielding. For example, a steric restriction appears when the dihedral angle, C7—C8—C9—O1, is ∼270°, as shown in Figure 8. This particular conformation corresponds to the point in Figure 9 at which the resonance of C7 is most isotropically shielded. For this situation, the C═O bond is perpendicular to the C7—C8 double bond. For this conformation, the p-orbital electron conjugation is destroyed, and the intermolecular hydrogen bonding between the hydroxyl group and the carbonyl oxygen is dramatically weakened, resulting in the significant shielding of C7. Indeed, the three principal values of C7 vary with conformation similarly, each having the maximal shielding when that dihedral angle is ∼270°. This joint variation of the chemical sift is reflected in the strong variation of the isotropic shift of C7 with conformation.

The principal values of the tensor for C8 and C9 show a dependence different from that of C7. The principal values of the tensor of these two sites often vary in the opposite sense. The net effect of this variation of the principal values is that the isotropic shift does not appear to change greatly with dihedral angle for C8 and C9. In particular, two principal values of the C9 CST vary strongly, but the isotropic shift changes little. These calculations suggest the importance of evaluating the principal values of chemical-shift tensors as a means to study the effect of structure on NMR properties.

Conclusions

Polymorphic piroxicam has been studied with solid-state NMR spectroscopy, X-ray diffraction, and DFT calculations. The isotropic ^{13}C chemical shifts of $\mathbf{P_I}$, $\mathbf{P_{II}}$, and **PM** have been completely assigned from CP/MAS spectra determined with and without suppression of signals of nonquaternary carbons. The principal values of the ^{13}C chemical-shift tensors of all the carbons of $\mathbf{P_I}$, $\mathbf{P_{II}}$, and **PM** have also been determined using the 2D-SUPER and DD-SUPER techniques. $^{13}C-^{1}H$ HETCOR spectra of **PM** indicate the appearance of two resonances for certain carbons (C1, C9, C11, C13, C15), which is NMR evidence that the asymmetric unit of the monohydrate contains two unique molecules.

The NMR analysis and DFT calculations demonstrate that the formation of **PM** from neutral piroxicam ($\mathbf{P_I}$/$\mathbf{P_{II}}$) must involve a proton transfer from the oxygen on C7 to the nitrogen N3 on the pyridine ring. Through-space dipolar correlations in the 2D-HETCOR NMR spectra suggest a structural model that involves hydrogen bonding of the oxygen at C9 to the water protons, as well as the previously proposed hydrogen bonding at the oxygen on C7. Alternatively, as suggested by Vogt et al.,[15] a combination of ^{15}N CP/MAS and ^{15}N dipolar-dephasing CP/MAS can be used to detect the protonation of the nitrogen atoms.

Calculations suggest that the principal values are more sensitive to changes of conformation than the isotropic chemical shifts. Evaluation of these parameters may provide a more detailed picture of the electronic structure and conformation in polymorphic materials.

Acknowledgment. This work was supported by the National Natural Science Foundation of China (21075057 and 20933009). C.D. acknowledges the support of the National Science Foundation under Grant CHE-0956006.

Supporting Information Available: PXRD data, ^{13}C CP/MAS spectra, ^{2}H MAS spectrum, and HETCOR spectra for $\mathbf{P_I}$, $\mathbf{P_{II}}$, and **PM**. This information is available free of charge via the Internet at http://pubs.acs.org.

References and Notes

(1) Guidance for Industry ANDAs: Pharmaceutical Solid Polymorphsim; U.S. Department of Health and Human Services, Food and Drug Administration, Center for Drug Evaluation and Research: Rockville, MD; July, 2007.

(2) Brittain, H. G.; Grant, D. J. W. *Effect of Polymorphism and Solid-State Solvation on Solubility and Dissolution Rate*; Marcel Dekker, Inc: New York, 1999.

(3) Byrn, S. R.; Pfeiffer, R. R.; Stowell, J. G. *Solid-State Chemistry of Drugs*, 2nd ed.; SSCI, Inc.: West Lafayette, IN, 1999.

(4) *The United States Pharmacopeia XXVII (USP27/NF22, 27th rev.)*; The United States Pharmacopeial Convention, Inc.: Rockville, MD, 2004.

(5) Sheth, A. R.; Bates, S.; Muller, F. X.; Grant, D. J. W. *Cryst. Growth Des.* **2004**, *4*, 1091.

(6) Bates, S.; Zografi, G.; Engers, D.; Morris, K.; Crowley, K.; Newman, A. *Pharm. Res.* **2006**, *23*, 2333.

(7) Childs, S. L.; Hardcastle, K. I. *Cryst. Growth Des.* **2007**, *7*, 1291.

(8) Bertoluzza, A.; Rossi, M.; Taddei, P.; Redenti, E.; Zanol, M.; Ventura, P. *J. Mol. Struct.* **1999**, *480−481*, 535.

(9) Taddei, P.; Torreggiani, A.; Simoni, R. *Biopolymers* **2001**, *62*, 68.

(10) Mehrens, S. M.; Kale, U. J.; Qu, X. *J. Pharm. Sci.* **2005**, *94*, 1354.

(11) Drebushchak, V. A.; Shakhtshneider, T. P.; Apenina, S. A.; Drebushchak, T. N.; Medvedeva, A. S.; Safronova, L. P.; Boldyrev, V. V. *J. Therm. Anal. Calorim.* **2006**, *84* (3), 643–649; **2006**, *26*, 643.

(12) Vrecer, F.; Srcic, S.; Smid-Korbar, J. *Int. J. Pharm.* **1991**, *68* (1−3), 35; **1991**, *68*, 35.

(13) Sheth, A. R.; Lubach, J. W.; Munson, E. J.; Muller, F. X.; Grant, D. J. W. *J. Am. Chem. Soc.* **2005**, *127*, 6641.

(14) Vrecer, F.; Vrbinc, M.; Meden, A. *Int. J. Pharm.* **2003**, *256*, 3.

(15) Vogt, F. G.; Clawson, J. S.; Strohmerier, M.; Edwards, A. J.; Pham, T. N.; Watson, S. A. *Cryst. Growth Des.* **2009**, *9*, 921.

(16) Kojic-Prodic, B.; Ruzic-Toros, Z. *Acta Crystallogr.* **1982**, *B32*, 2948.

(17) Bordner, J.; Richards, J. A.; Weeks, P.; Whipple, E. B. *Acta Crystallogr., Sect C: Cryst. Struct. Commun.* **1984**, *40*, 989.

(18) Reck, G.; Dietz, G.; Laban, G.; Gunther, W.; Bammier, G.; Hohne, E. *Pharmazie* **1988**, *43*, 477.

(19) Harper, J. K.; Doebbler, J. A.; Jacques, E.; Grant, D. M.; Von Dreele, R. B. *J. Am. Chem. Soc.* **2010**, *132*, 2928.

(20) Harper, J. K.; Grant, D. M.; Zhang, Y.; Lee, P. L.; von Dreele, R. B. *J. Am. Chem. Soc.* **2006**, *128*, 1547.

(21) Heider, E. M.; Harper, J. K.; Grant, D. M. *Phys. Chem. Chem. Phys.* **2007**, *9*, 6083.

(22) Olejniczak, S.; Mikula-Pachoczyk, J.; Hughes, C. E.; Potrzebowski, M. J. *J. Phys. Chem.* **2008**, *122*, 1586.

(23) Olejniczak, S.; Potzebowski, M. J. *Org. Biomol. Chem.* **2004**, *2*, 7.

(24) Smith, J.; MacMamara, E.; Raftery, D.; Borchardt, T.; Byrn, S. *J. Am. Chem. Soc.* **1998**, *120*, 11710.

(25) Smith, J.; Xu, W.; Raftery, D. *J. Phys. Chem. B* **2006**, *110*, 7766.

(26) Bai, S.; Wang, W.; Dybowski, C. R. *Anal. Chem.* **2010**, *82*, 4917.

(27) Berendt, R. T.; Sperger, D. M.; Munson, E. J.; Isbester, P. K. *Trends Anal. Chem.* **2006**, *25*, 977.

(28) Geppi, M.; Mollica, G.; Borsacchi, S.; Veracini, C. A. *Appl. Spectrosc. Rev.* **2008**, *43*, 202.

(29) Opella, S. J.; Frey, M. H. *J. Am. Chem. Soc.* **1979**, *101*, 5854.

(30) Sheth, A. R.; Zhou, D.; Muller, F. X.; Grant, D. J. W. *J. Pharm. Sci.* **2004**, *93*, 3013.

(31) Bennett, A. E.; Rienstra, C. M.; Auger, M.; Lakshmi, K. V.; Griffin, R. G. *J. Chem. Phys.* **1995**, *103*, 6951.

(32) van Rossum, B.-J.; Forster, H.; de Groot, H. J. M. *J. Magn. Reson.* **1997**, *124*, 516.

(33) Bielecki, A.; Kolbert, A. C.; Levitt, M. H. *Chem. Phys. Lett.* **1989**, *155*, 341.

(34) Lee, M.; Goldburg, W. I. *Phys. Rev. A* **1965**, *140*, 1261.

(35) Alderman, D. W.; McGeorge, G.; Hu, J. Z.; Pugmire, R. J.; Grant, D. M. *Mol. Phys.* **1998**, *95*, 1113.

(36) Antzukin, O. N.; Shekar, S. C.; Levitt, M. H. *J. Magn. Reson. Ser. A* **1995**, *115*, 7.

(37) Chan, J. C. C.; Tycko, R. *J. Chem. Phys.* **2003**, *118*, 8378.

(38) Liu, S.-F.; Mao, J.-D.; Schmidt-Rohr, K. *J. Magn. Reson.* **2002**, *155*, 15.

(39) Dixon, W. T. *J. Magn. Reson.* **1981**, *44*, 220.

(40) Dixon, W. T. *J. Chem. Phys.* **1982**, *77*, 1800.

(41) Liu, W.; Wang, D. W.; Wang, W.; Bai, S.; Dybowski, R. C. *J. Magn. Reson.* **2010**, *206*, 177.

(42) Baerends, E. J.; Autschbach, A.; Berces, A.; Bickelhaupt, F. M.; Bo, C.; Boerrigter, P. M.; Cavallo, L.; Chong, D. P.; Deng, L.; Dickson, R. M.; Ellis, D. E.; van Faassen, M.; Fan, L.; Fischer, T. H.; Fonseca Guerra, C.; van Gisbergen, S. J. A.; Groeneveld, J. A.; Gritsenko, O. V.; Gruning, M.; Harris, F. E.; van den Hoek, P.; Jacob, C. R.; Jacobsen, H.; Jensen, L.; van Kessel, G.; Kootstra, F.; van Lenthe, E.; McCormack, D. A.; Michalak, A.; Neugebauer, J.; Osinga, V. P.; Patchkovskii, S.; Philipsen, P. H. T.; Post, D.; Pye, C. C.; Ravenek, W.; Ros, P. S., P. R. T.; Schreckenbach, G.; Snijders, J. G.; Sola, M.; Swart, M.; Swerhone, D.; te Velde, G.; Vernooijs, P.; Versluis, L.; Visscher, L.; Visser, O.; Wang, F.; Wesolowski, T. A.; van Wezenbeek, E.; Wiesenekker, G. *ADF2009.01, SCM, Theoretical Chemistry*; Vrije Universiteit: Amsterdam, The Netherlands. URL http://www.scm.com.

(43) Schreckenbach, G.; Ziegler, T. *J. Phys. Chem.* **1995**, *99*, 606.

(44) Krykunov, M.; Ziegler, T.; van Lenthe, E. *Int. J. Quantum Chem.* **2009**, *109*, 1676.

(45) Wolff, S. K.; Ziegler, T. *J. Chem. Phys.* **1998**, *109*, 895.

(46) Frisch, M. J.; Trucks, G. W.; Schlegel, H. B.; Scuseria, G. E.; Robb, M. A.; Cheeseman, J. R.; Montgomery, J.; Vreven, J. A. T.; Kudin, K. N.; Burant, J. C.; Millam, J. M.; Iyengar, S. S.; Tomasi, J.; Barone, V.; Mennucci, B.; Cossi, M.; Scalmani, G.; Rega, N.; Petersson, G. A.; Nakatsuji, H.; Hada, M.; Ehara, M.; Toyota, K.; Fukuda, R.; Hasegawa, J.; Ishida, M.; Nakajima, T.; Honda, Y.; Kitao, O.; Nakai, H.; Klene, M.; Li, X.; Knox, J. E.; Hratchian, H. P.; Cross, J. B.; Bakken, V.; Adamo, C.; Jaramillo, J.; Gomperts, R.; Stratmann, R. E.; Yazyev, O.; Austin, A. J.; Cammi, R.; Pomelli, C.; Ochterski, J. W.; Ayala, P. Y.; Morokuma, K.; Voth, G. A.; Salvador, P.; Dannenberg, J. J.; Zakrzewski, V. G.; Dapprich, S.; Daniels, A. D.; Strain, M. C.; Farkas, O.; Malick, D. K.; Rabuck, A. D.; Raghavachari, K.; Foresman, J. B.; Ortiz, J. V.; Cui, Q.; Baboul, A. G.; Clifford, S.; Cioslowski, J.; Stefanov, B. B.; Liu, G.; Liashenko, A.; Piskorz, P.; Komaromi, I.; Martin, R. L.; Fox, D. J.; Keith, T.; Al-Laham, M. A.; Peng, C. Y.; Nanayakkara, A.; Challacombe, M.; Gill, P. M. W.; Johnson, B.; Chen, W.; Wong, M. W.; Gonzalez, C.; Pople, J. A. Gaussian, Inc.: Wallingford, CT, 2004.

(47) Yu, L.; Stephson, G. A.; Mitchell, C. A.; Bunnell, C. A.; Snorek, S. V.; Bowyer, J. J.; Borchardt, T. B.; Stowell, J. G.; Byrn, S. R. *J. Am. Chem. Soc.* **2000**, *122*, 585.

(48) Harper, J. K.; Grant, D. M. *J. Am. Chem. Soc.* **2000**, *122*, 3708.

(49) Wu, G.; Freure, C. J.; Verdurand, E. *J. Am. Chem. Soc.* **1998**, *120*, 13187.

(50) Robbins, A. J.; Ng, W. T.; Jochym, D.; Keal, T. W.; Clark, S. J.; Tozer, D. J.; Hodgkinson, P. *Phys. Chem. Chem. Phys.* **2007**, *9*, 2389.

(51) Sakellariou, D.; Brown, S. P.; Lesage, A.; Hediger, S.; Bardet, M.; Meriles, C. A.; Pines, A.; Emsley, L. *J. Am. Chem. Soc.* **2003**, *125*, 4376.

(52) Antzutkin, O. N.; Shekar, S. C.; Levitt, M. H. *J. Magn. Reson.* **1998**, *135*, 144.

(53) Gerstein, B. C.; Dybowski, C. R. *Transient Techniques in NMR of Solids*; Academic Press: Orlando, FL, 1985.

(54) Gu, Z.; McDermott, A. E. *J. Am. Chem. Soc.* **1993**, *115*, 4282.

(55) Gu, Z.; Zambrano, R.; McDermott, A. E. *J. Am. Chem. Soc.* **1994**, *111*, 6368.

(56) Wei, Y. F.; Lee, D. K.; Rammamoorthy, A. *J. Am. Chem. Soc.* **2001**, *123*, 6118.

JP1084444